DOI 10.1007/s10717-023-00565-x
Glass and Ceramics, Vol. 80, Nos. 3 – 4, July, 2023 (Russian Original, Nos. 3 – 4, March – April, 2023)

UDC 666.3:544.6.018.42-16

ELECTRICAL CHARACTERISTICS OF BISMUTH-CONTAINING CERIUM OXIDE

I. V. Sudzhanskaya[1] and V. S. Sotnikova[1, 2]

Translated from *Steklo i Keramika*, No. 3, pp. 26 – 32, March, 2023.

Original article submitted August 26, 2022.

The ceramics $Ce_{0.9}Bi_{0.1}O_{2-\delta}$ was obtained by solid-phase synthesis. It is shown that the obtained samples possess a cubic fluorite structure with the space symmetry group *Fm*3*m*. The electrical properties of the solid solution $Ce_{0.9}Bi_{0.1}O_{2-\delta}$ solid solution were investigated by means of ac impedance spectrometry. The activation energy of electric conduction falls into two regions – 0.51 eV (400 – 680°C) and 1.6 eV (680 – 800°C); dielectric relaxation is activated at 0.88 eV.

Keywords: cerium oxide, ionic conductivity, impedance spectroscopy, dielectric relaxation.

INTRODUCTION

Cerium-oxide based ceramic doped with rare-earth and (or) alkaline-earth elements finds owing to its high ionic conductivity application in medium-temperature solid electrolytes of solid-oxide fuel cells [1 – 3], oxygen sensors [4, 5], catalysts [6, 7], and elsewhere.

Numerous investigations have shown that Gd-, Sm-, and Y-doping of cerium oxide effects production of ceramics with heightened oxygen ion conductivity in the medium temperature range [8–15]. However, the sintering temperature of such a ceramic exceeds 1500°C, which results in grain enlargement and, consequently, growth of the resistance along grain boundaries and deterioration in mechanical properties [16, 17].

It is well known that on account of a high concentration of oxygen vacancies and high mobility of anions Bi_2O_3 with fluorite structure has high ionic conductivity and low sintering temperature [18, 19].

The preparation of a single-phase CeO_2–Bi_2O_3 solution with fluorite structure depends on the synthesis parameters and the sintering temperature [19 – 23].

The authors of [19] investigated the CeO_2–Bi_2O_3 system obtained by means of a solid-phase reaction at Bi_2O_3 concentration 0 to 40 mol.% and annealing temperature 820°C. Fluorite structure was not detected.

The solid solution $(CeO_2)_{1-x}(BiO_{1.5})_x$, where $0 < x < 0.50$, was obtained by means of low-temperature hydrothermal synthesis [24]. All the resulting solutions possessed a single-phase cubic fluorite structure. The conductivity of the composition $(CeO_2)_{0.5}(BiO_{1.5})_x$ reached 3.8×10^{-4} S/cm at 1400°C. The activation energy of this system was equal to 1.17 eV.

A sintering temperature reduction in doped ceramic based on cerium dioxide to 1250°C is displayed in [25]. Doping Bi_2O_3 to 2% cerium oxide doped with Gd (20%) effects the formation of a fluorite structure with a higher density and electrical conductivity in the range 550–800°C (1.1×10^{-2} – 1.1×10^{-2} S/cm).

The main process of increasing the electrical conductivity in doped cerium dioxide is the diffusion of oxygen ions through oxygen vacancies. The activation energy of ionic conduction is the sum of the migration energy E_m and the energy required to create a mobile free oxygen vacancy that promotes oxygen migration E_O [26]. Ionic displacements resulting from the migration of oxygen ions result in the appearances of a dipole moment and a dielectric relaxation process [27]. The method for measuring dielectric relaxation is the dielectric loss tangent method, or dissipation of electrical energy, the cause of which is the reorientation of defects induced by an electric field [28].

The purpose of the present work was to investigate the electrical conductivity and dielectric relaxation of $CeO_2Bi_2O_3$ ceramics.

[1] Belgorod National Research University, Belgorod, Russia (e-mail: sudzhanskaya@bsu.edu.ru).
[2] V. G. Shukhov Belgorod State Technological University, Belgorod, Russia (e-mail: sotnikova_v@bsu.edu.ru).

OBTAINING SAMPLES AND METHODS OF INVESTIGATION

Samples of the solid solution $Ce_{0.9}Bi_{0.1}O_{2-\delta}$ were obtained by the solid phase reaction method. The composition $0.9CeO_2$–$0.1Bi_2O_3$, taken in stoichiometric ratio, was stirred for 2 h in an agate mortar with the addition of ethyl alcohol. The mixture thus obtained was dried at 373 K for 1 h. The obtained powders were compacted, by means of biaxial pressing under 25 MPa, in the form of tablets with diameter 12 mm and thickness 1 mm. The samples were sintered for 3 h in air at 1073 K.

The phase composition of the synthesized samples was determined using a Rigaku Ultima IV x-ray diffractometer.

The relative density ρ was calculated as the ratio of the apparent density ρ_{exp} to the theoretical density ρ_{the} according to the correlation

$$\rho = \frac{\rho_{exp}}{\rho_{th}} \times 100\%. \quad (1)$$

The theoretical density was determined from the crystallographic equation [30]

$$\rho = \frac{Z\sum_i \nu_i M_i}{a^3 N_A}, \quad (2)$$

where ν_i is the stoichiometric coefficient; Z is the number of formula units per unit cell (i.e. four for cerium with the fluorite structure); M_i is the molar mass of an atom, $g \cdot mol^{-1}$; a is a lattice parameter; N_A is the Avogadro constant, equal to 6.022×10^{23} mol^{-1}.

The electrical characteristics of the obtained samples were measured on a Novocontrol Concept 43 impedance spectrometer. To do this, silver paste was pre-applied to the ends of the sample on both sides.

RESULTS AND DISCUSSION

Figure 1 shows an x-ray diffraction pattern of a $Ce_{0.9}Bi_{0.1}O_{2-\delta}$ ceramic sample sintered at 800°C for 3 h, belonging to a cubic fluorite structure with space symmetry group $Fm3m$ (225) and crystal lattice parameters $a = b = c =$ 5.3874 Å corresponding to CeO_2.

The relative density of the sintered ceramic was 80% of the theoretical density of 7.27 g/cm^3.

Figure 2 shows the impedance spectrum obtained at 300 K, where the real part 29 Z' of the total impedance depends on the imaginary part Z''.

Three sections are observed in the impedance spectrum: high-frequency arc (cyclic frequency $\omega = 2\pi f$), related with the polarization in the bulk of the grain; mid-frequency region associated with polarization along grain boundaries; low-frequency region due to the influence of the electrode/electrolyte interface. In the present case the third section (the influence of the electrodes is neglected) will not be considered. The inset in Fig. 2, following the brick-row model [29], shows standard equivalent circuits containing a constant phase element (CPE = Q) [12].

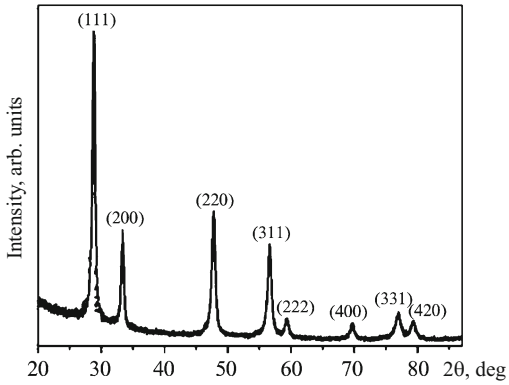

Fig. 1. X-ray diffraction pattern of $Ce_{0.9}Bi_{0.1}O_{2-\delta}$.

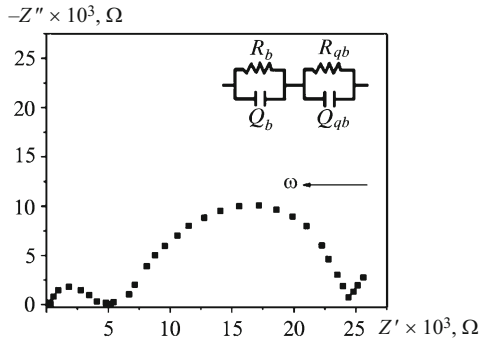

Fig. 2. Impedance spectrum of ceramic $Ce_{0.9}Bi_{0.1}O_{2-\delta}$ obtained at 300 K.

Impedance spectroscopy is necessary for studying the transport properties of materials. The electric and transport properties can be analyzed using the equations [30]:

$$Z^* = Z' + jZ''; \quad (3)$$

$$\varepsilon' = \frac{Z''}{Z'^2 + Z''^2}\frac{1}{\omega C_0}; \quad \varepsilon'' = \frac{Z'}{Z'^2 + Z''^2}\frac{1}{\omega C_0}, \quad (4)$$

where ε′ is the real part of the permittivity; ε″ is the imaginary part of the permittivity; j is the imaginary unit; $C_0 = \varepsilon_0 A/t$ – geometric capacitance; $\varepsilon_0 = 8.85 \times 10^{-12}$ F/m; A — area of surface; and, t is the sample thickness.

The ac conductance is calculated according to the expression

$$\sigma = \frac{Z'}{Z'^2 + Z''^2}\frac{t}{A}. \quad (5)$$

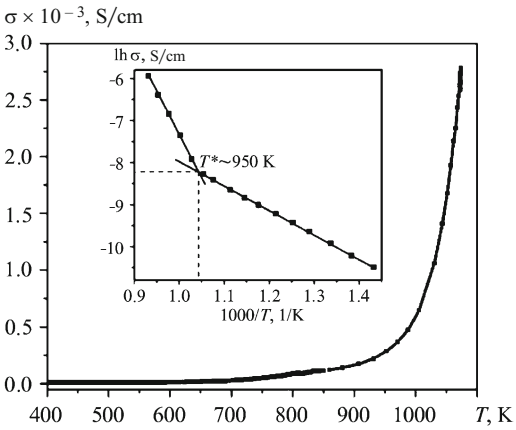

Fig. 3. Temperature dependence of the electrical conductivity of $Ce_{0.9}Bi_{0.1}O_{2-\delta}$ ceramics.

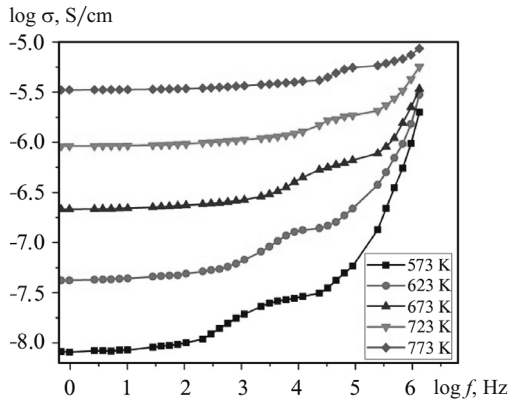

Fig. 4. Logarithmic curves of the electrical conductivity spectrum versus the frequency for the ceramics $Ce_{0.9}Bi_{0.1}O_{2-\delta}$ at different temperatures.

The activation energy of the specific electrical conductivity is determined by the Arrhenius relation

$$\sigma = \sigma_0 e^{-\frac{U}{kT}}, \qquad (6)$$

where σ_0 is the pre-exponential factor; k is the Boltzmann constant; T is temperature; and, U is activation energy.

The temperature dependence of electrical conductivity is shown in Fig. 3, according to which an exponential increase in electrical conductivity is observed with increasing temperature. The inset in Fig. 3 shows the function $\ln\sigma\,(1/T)$ for the ceramic $Ce_{0.9}Bi_{0.1}O_{2-\delta}$, calculated from the tangent of the slope angle, on which two linear sections are observed, the intersection of these sections on the graph is indicated by the symbol T^*. The activation energy was equal to 0.51 eV in the low temperature range 400 – 680°C (about 950 K) and 1.6 eV in the range 680 – 800°C, respectively, which is associated with the predominance of the electronic type conductivity in this temperature range, as is characteristic of pure CeO_2 above 550°C [2].

The frequency dependence of the conductivity spectrum of the $Ce_{0.9}Bi_{0.1}O_{2-\delta}$ system at different temperatures is shown in Fig. 4.

The obtained frequency spectra of electrical conductivity demonstrate a strong dependence on temperature. In the low-temperature range, the electrical conductivity increases exponentially.

As temperature increases, the observed steps of the frequency dispersion at mid-range frequencies shift to high frequencies, which is associated with the relaxation of grain boundaries [31]. The large dispersion obtained in the intermediate frequency range of the conductivity plot can also be associated with the mobility of dimer associates, which do not participate in the conductivity of oxide ions but contribute to the permittivity [32].

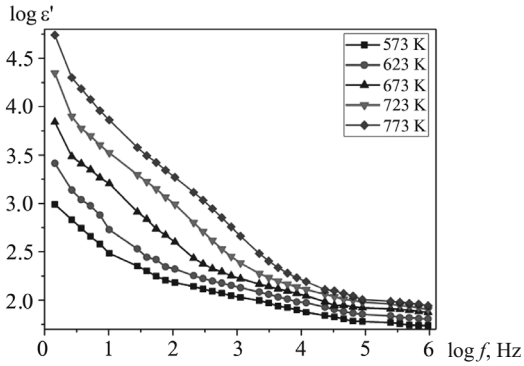

Fig. 5. Logarithmic curves of the real part of the permittivity of the $Ce_{0.9}Bi_{0.1}O_{2-\delta}$ solid solution versus frequency.

The frequency dependence of the real part of the permittivity of $Ce_{0.9}Bi_{0.1}O_{2-\delta}$ ceramics, obtained at different temperatures, is shown in Fig. 5.

At low frequencies the increase is associated with the polarization of oxygen ions at the electrode–electrolyte interface, since oxygen ions hop in the direction of the field and accumulate in places with a high energy barrier, which effects higher capacitance in the direction of the field after hopping through places with low energy barrier. At high frequencies, the periodic reversal of the field occurs so rapidly that there are no excessive hops of ions in the direction of the field. The capacitive effect disappears in regions with a high energy barrier, which reduces the contribution of charge carriers to the permittivity and manifests itself as reduction with increasing frequency [33]. The observed frequency dispersion shifts with increasing temperature, which is associated with the effect of grain boundaries.

The temperature dependence of the real part of the dielectric permittivity and the dielectric loss tangent $\tan\delta$ of $Ce_{0.9}Bi_{0.1}O_{2-\delta}$ ceramics is shown in Fig. 6.

A step in the temperature range of 450 – 650 K is observed on the temperature dependence of the permittivity. An

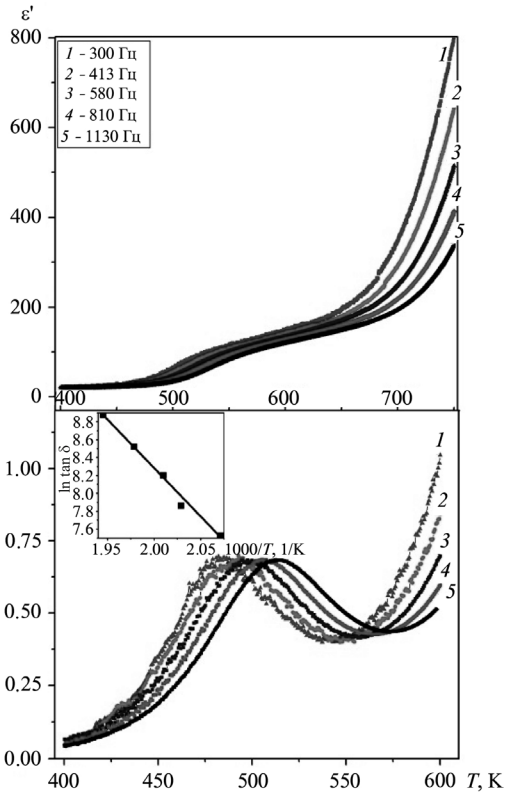

Fig. 6. Temperature dependence of the permittivity and dielectric loss tangent of $Ce_{0.9}Bi_{0.1}O_{2-\delta}$ ceramics.

analysis of the dielectric loss spectrum shows that at 475 K and 300 Hz a peak is observed; as frequency increases, the peak shifts towards higher temperatures — dielectric relaxation associated with the migration of oxygen vacancies in the system $Ce_{0.9}Bi_{0.1}O_{2-\delta}$.

The activation energy U of the dielectric relaxation process is determined from the Arrhenius law

$$\tau = \tau_0 \exp\left(\frac{-U}{kT}\right), \quad (7)$$

where τ_0 is a pre-exponential factor. The relaxation time was determined using the expression

$$\tau = \frac{1}{2\pi f}, \quad (8)$$

where f is the frequency. The activation energy of the dielectric relaxation process in $Ce_{0.9}Bi_{0.1}O_{2-\delta}$ ceramic was equal to 0.88 eV.

CONCLUSIONS

Samples of the compositions $Ce_{0.9}Bi_{0.1}O_{2-\delta}$ were obtained by the method of reactions in the solid phase. The sintering temperature was equal to 800°C and the exposure time 3 h. The x-ray method showed that the ceramics had a cubic lattice with a fluorite structure and symmetry space group $Fm3m$ belonging to CeO_2.

Using impedance spectrometry on alternating current, it was found that the activation energy of electrical conductivity has two sections — 0.51 eV (400 – 680°C) and 1.6 eV (680 – 800°C), which is associated with the predominance of the electronic type of conductivity in this temperature range, characteristic of pure CeO_2.

The spectra of electrical conductivity and dielectric permittivity show strong dispersion in the mid-frequency range associated with relaxation along grain boundaries. The activation energy of the dielectric relaxation process was determined to be 0.88 eV, which is associated with the migration of oxygen vacancies.

The article was prepared as part of the development program of the National Research University "BelSU" for 2021 – 2030. (The program of strategic academic leadership "Priority-2030") using the equipment of the Center for Collective Use "Technologies and Materials of the National Research University BelSU."

REFERENCES

1. Y. Zhang, R. Knibbe, J. Sunarso, and Y. Zhong, "Recent progress on advanced materials for solid-oxide fuel cells operating below 500°C," *Adv. Mater.*, **29**, 1700132 (2017). URL: https://doi.org/10.3390/inorganics7100118
2. H. Inaba and H. Tagawa, "Review ceria-based solid electrolytes," *Solid State Ionics*, **83**, 1 – 16 (1996). URL: https://doi.org/10.1016/0167-2738(95)00229-4
3. B. Wang, B. Zhu, S. Yun, and W. Zhang, "Fast ionic conduction in semiconductor $CeO_{2-\delta}$ electrolyte fuel cells," *NPG Asia Mater.*, **11**, 51 (2019). URL: https://doi.org/10.1038/s41427-019-0152-8
4. E. L. Brosha, R. Mukundan, D. R. Brown, and F. H. Garzon, "Development of ceramic mixed potential sensors for automotive applications," *Solid State Ionics*, **148**, 61 – 69 (2002). URL: https://doi.org/10.1016/S0167-2738(02)00103-0
5. U. Nigge, H. D. Wiemhofer, E. W. J. Romer, and H. J. M. Bouwmeester, "Composites of $Ce_{0.8}Gd_{0.2}O_{1.9}$ and $Gd_{0.7}Ca_{0.3}CoO_3$ das oxygen permeable membranes for exhaust gas sensor," *Solid State Ionics*, **146**(1 – 2), 163 (2002). URL: https://doi.org/10.1016/S0167-2738(01)00984-5
6. D. He, H. Hao, D. Chen, and J. Liu, "Synthesis and application of rare-earth elements (Gd, Sm, and Nd) doped ceria-based solid solutions for methyl mercaptan catalytic decomposition," *Catalysis Today*, **281**, 559 – 565 (2017). URL: https://doi.org/10.1016/j.cattod.2016. 06.022
7. A. Vita Catalytic, "Applications of CeO_2-based materials," *Catalysts*, **10**, 576 (2020). URL: https://doi.org/10.3390/catal10050576
8. Y. Zhang, Ch. Lenser, and N. H. Menzler, "Comparison of solid oxide fuel cell (SOFC) electrolyte materials for operation at 500°C," *Solid State Ionics*, **344**, 115138 (2020).
9. P. Ramos-Alvarez, M. E. Villafuerte-Castrejón, G. González, and M. Cassir, "Ceria-based electrolytes with high surface area and improved conductivity for intermediate temperature solid oxide fuel cells," *J. Mater. Sci*., **52**(1), 519–532 (2017).

10. J. Wang, S. Chen Xie, et al., "Bismuth tungstate/neodymium-doped ceria composite electrolyte for intermediate-temperature solid oxide fuel cell: Sintering aid and composite effect," *J. Power Sources*, **428**, 105 – 114 (2019).
11. H. Hu, H. Yan, and Z. Chen, "Sintering and electrical properties of $Ce_{0.8}Y_{0.2}O_{1.9}$ powders prepared by citric acid-nitrate low-temperature combustion process," *J. Power Sources*, **163**, 409 – 414 (2006).
12. L. Bouria, B. Bakiz, A. Benlhachemi, et al., "Electrical properties of a CeO_2–Bi_2O_3, mix system elaborated at 600°C," *Adv. Mater. Sci. Eng*., No. 2, 1 – 11 (2012). DOI:10.1155/2012/452383
13. G. Accardo, D. Frattini, H. C. Ham, and S. P. Yoon, "Direct addition of lithium and cobalt precursors to $Ce_{0.8}Gd_{0.2}O_{1.95}$ electrolytes to improve microstructural and electrochemical properties in IT-SOFC at lower sintering temperature," *Ceram. Int*., **45**(7), pt B, 9348 – 9358 (2019).
14. D. J. L. Brett, A. Atkinson, N. P. Brandon, and S. J. Skinner, "Intermediate temperature solid oxide fuel cells," *Chem. Soc. Rev.*, **37**, 1568 – 1578 (2008).
15. D. Liu, D. Ding, M. Liu, et al., "High-performance, ceria-based solid oxide fuel cells fabricated at low temperatures," *J. Power Sources*, **241**, 454 – 459 (2013).
16. G. Accardo, D. Frattini, H. C. Ham, and J. H. Han, "Improved microstructure and sintering temperature of bismuth nano-doped GDC powders synthesized by direct sol-gel combustion," *Ceram. Int*., **44**, 3800 – 3809 (2018). URL: https://doi.org/10.1016/j.ceramint.2017.11.165
17. G. Accardo, D. Frattini, H. C. Ham, and S. P. Yoon, "Direct addition of lithium and cobalt precursors to $Ce_{0.8}Gd_{0.2}O_{1.95}$ electrolytes to improve microstructural and electrochemical properties in IT-SOFC at lower sintering temperature," *Ceram. Int*., **45**, 9348 – 9358 (2019). URL: https://doi.org/10.1016/j.ceramint.2018.07.209
18. S. Sanna, V. Esposito, M. Christensen, and N. Pryds, "High ionic conductivity in confined bismuth oxide-based heterostructures," *Apl. Mater.*, **4**, 12110 (2016). URL: https://doi.org/10.1063/1.4971801
19. X. L. Chen and W. Eysel, "The stabilization of β-Bi_2O_3 by CeO_2," *J. Solid State Chem*., **127**, 128 – 130 (1996).
20. L. Bourja, B. Bakiz, A. Benlhachemi, et al., "Structural and Raman vibrational studies of CeO_2–Bi_2O_3 oxide system," *Adv. Mater. Sci. Eng*., No. 2. 1 – 4 (2009).
21. I. V. Zagaynov, S. V. Fedorov, A. A. Konovalov, and O. S. Antonova, "Perspective ceria-based solid solution of $Gd_xBi_{0.2-x}Ce_{0.8}O_2$," *Mater. Lett*. **203**. 9 – 12 (2017).
22. Z.-C. Li, H. Zhang, and B. Bergman, "Synthesis and characterization of nanostructured Bi_2O_3-doped cerium oxides fabricated by PVA polymerization process," *Ceram. Int*., **34**, 1949 – 1953 (2008).
23. S. Dikmen, P. Shuk, and M. Greenblatt, "Hydrothermal synthesis and properties of $Ce_{1-x}Bi_xO_{2-\delta}$ solid solutions," *Solid State Ionics*, **11**, 299 – 307 (1998).
24. G. Li, L. Li, S. Feng, Yao, et al., "An Effective Synthetic Route for a Novel Electrolyte: Nanocrystalline Solid Solution of $(CeO_2)_{1-x}(BiO_{1.5})_x$," *Adv. Mater.*, **11**(2), 146 – 149 (1999).
25. G. Accardo, L. Spiridigliozzi, G. Dell'Agli, et al., "Morphology and structural stability of bismuth-gadolinium Co-doped ceria electrolyte nanopowders," *Inorganics*, **7**, 118 (2019). URL: https://doi.org/10.3390/inorganics7100118
26. K. P. Padmasree, R. A. Montalvo-Lozano, S. M. Montemajor, and A. F. Fuentes, "Electrical conduction and dielectric relaxation process in $Ce_{0.8}Y_{0.2}O_{1.9}$ electrolyte system," *J. Alloys Compds*., **509**, 8584 – 8589 (2011).
27. R. Gerhardt, "Impedance and dielectric spectroscopy revisited: Distinguishing localized relaxation from long-range conductivity," *J. Phys. Chem. Solids*, **55**, 1491 – 1506 (1994). URL: https://doi.org/10.1016/0022-3697(94)90575-4
28. M. Kurumada, H. Hara, and E. Iguchi, "Oxygen vacancies contributing to intragranular electrical conduction of yttria-stabilized zirconia (YSZ) ceramics," *Acta Mater.*, **53**(18), 4839 – 4846 (2005). URL: https://doi.org/10.1016/j.actamat.2005.06.027
29. N. J. Kidner, N. H. Perry, T. O. Mason, "The brick lauer model revisited: Introducing the nanj-grain composite model," *J. Am. Ceram. Soc*., **91**(6), 1733 – 1746 (2008). URL: https://doi.org/10.1111/j.1551-2916.2008.02445.x
30. S. Ramesh, "Transport properties of Sm doped CeO_2 ceramics," *Proc. Appl. Ceram*., **15**(4), 366 – 373 (2021). DOI: 10.2298/PAC2104366E
31. A. Pimenov, J. Ullrich, P. Lunkenheimer, et al., "Ionic conductivity and relaxations in ZrO_2–Y_2O_3 solid solutions," *Solid State Ionics*, **109**(1 – 2), 111 – 118 (1998). URL: https://doi.org/10.1016/S0167-2738(98)00082-4
32. H. Yamamura, S. Takeda, and K. Kakinuma, "Relationship between oxide-ion conductivity and dielectric relaxation in Sm-doped CeO_2," *Solid State Ionics*, **178**(13 – 14), 889 – 893 (2007). URL: https://doi.org/10.1016/j.ssi.2007.04.013
33. K. P. Padmasree and D. K. Kanchan, "Conductivity and dielectric studies on $20CdI_2 - 80[xAg_2O - y(0.7V_2O_5 - 0.3B_2O_3)]$ super ion conducting system where $1 \le x/y \le 3$," *J. Non-Cryst. Solids*, **352**(36 – 37), 3841 – 3848 (2006). URL: https://doi.org/10.1016/j.jnoncrysol.2006.06.012